Appl Phys A (2009) 95: 889–898
DOI 10.1007/s00339-009-5093-6

Applied Physics A
Materials Science & Processing

A mechanism for the formation of annealed compact oxide layers at the interface between anodic titania nanotube arrays and Ti foil

Chien-Chon Chen · Wen C. Say · Sheng-Jen Hsieh · Eric Wei-Guang Diau

Received: 9 June 2008 / Accepted: 29 December 2008 / Published online: 4 February 2009

Abstract We propose a mechanism for the growth of crystalline anodic titanium-oxide (ATO) nanochannel arrays based on thermodynamic considerations and structural imperfections. Both amorphous and crystalline ATO films were obtained from the anodization of a titanium foil. Amorphous ATO nanotubes have a single-layer form, which makes them inefficient for use in photo-catalytic and solar-cell applications. Annealed ATO nanotubes are considered non-stoichiometric if the effect of oxygen partial pressure on the composition is significant. The driving force behind growing crystalline ATO nanotubes is the drawing of oxygen from the atmosphere to the oxygen site, which consequently decreases the concentration of oxygen vacancies in the anatase phase. The small ionization energies of titanium ions produce the stoichiometric defects. A diagram showing Gibbs energy and Kroger–Vink notation to indicate the strong influence of the non-stoichiometric ATO structure is deduced.

C.-C. Chen · E.W.-G. Diau (✉)
Department of Applied Chemistry and Institute of Molecular Science, National Chiao Tung University, Hsinchu 30010, Taiwan
e-mail: diau@mail.nctu.edu.tw
Fax: +886-03-5723764

C.-C. Chen
Department of Energy and Resources, National United University, Miaoli 36003, Taiwan

W.C. Say
Department of Materials & Mineral Resources Engineering, National Taipei University of Technology, Taipei 10643, Taiwan

S.-J. Hsieh
Department of Engineering Technology and Department of Mechanical Engineering, Texas A&M University, College Station, TX 77843-3367, USA

PACS 61.46.Fg · 64.70.Nd · 61.50.Ah

1 Introduction

Nanoporous films with large surface-to-volume ratios have attracted much attention [1–3]. Ordered nanochannel films with uniform nanopore sizes are formed on active metals such as Al, Zr, Nb, Sn, W, Hf, and Ti on anodization [4–10]. Of anodic oxide nanochannel arrays of various types, thin films of anodic titanium oxide (ATO) possess great thermal and chemical stability, which makes them useful for catalytic [11], gas-sensing [12], self-cleaning [13], and dye-sensitized solar-cell [10, 14–16] applications.

A compact ATO film is readily obtained with a dilute solution of sulfuric acid and an anti-corrosion film to maintain an enduring exterior [17]. Zwilling [18] described the fabrication of ATO nanotube arrays, and Grimes and co-workers [19–21] presented greater details. According to their approach, the lengths of ATO nanotubes were controlled with an electrolyte solution containing fluoride ions: the tube length was ∼0.5 μm in a HF-based aqueous electrolyte and ∼7 μm in a NaF or KF aqueous electrolyte. Macak et al. [22] made the first nanotubes with a large aspect ratio in organic non-aqueous and fluoride-based electrolytes. The length of the ATO nanotubes attained was 134 μm [23], 220 μm [16], and 1000 μm [24].

The initial phase of ATO is amorphous, which is inefficient for photo-catalytic and solar-cell applications. This problem is ameliorated on thermal treatments; Varghese et al. [25] showed that amorphous ATO crystallizes to an anatase phase at temperatures between 280 and 450°C and enters the rutile phase between 480 and 620°C. When titanium specimens are anodized or thermally treated, titanium oxides or layers comprise not a single component, but the

ratio of titanium to oxygen varies layer by layer. The components in ATO layers are hence more appropriately described as TiO_{2-x}, with $0 < x < 1$. According to Mantzila and Prodromidis [26], the native layers of Ti_2O_3 and TiO are formed at the interface between the anodic film of TiO_2 and the Ti substrate, and TiO_x layers are produced between TiO and Ti; TiO_x might there consist of Ti_3O_5 and Ti_4O_7. According to their assumption, the oxide layers above Ti are sequentially TiO_x, TiO, and TiO_2, but a thermochemical table lists the thermodynamically stable titanium oxides as TiO, Ti_2O_3, Ti_3O_5, and Ti_4O_7 [27]. Through a thermodynamic calculation we thus correct the order of the oxide layers on Ti to TiO, Ti_2O_3, Ti_3O_5, Ti_4O_7, and TiO_2. We here describe annealing the ATO film with nanochannel structures to attain the anatase TiO_2 phase, including the deduction of thermodynamic stability and corresponding non-stoichiometric reactions, and we elucidate the relations between the order and disorder transformations during the formation of ATO nanochannel arrays.

2 Experiments

2.1 Electro-polishing

A piece ($2 \times 1 \times 0.01$ cm^3) of titanium foil (purity 99.7%) was annealed in a furnace in air at 800°C for 1 h to obtain an α-phase microstructure that was abraded (#1500 grit SiC paper). Electro-polishing (EP) at 15°C with applied voltage 40 V for 5 min yielded flat surfaces of α-titanium from a Pt cathode (2 cm^2). The electrolyte polish was composed of $HClO_4$ (5% vol), $HOCH_2CH_2OC_4H_9$ (53% vol) and H_3COH (42% vol).

2.2 Anodization

The electro-polished α-Ti anode and the same cathode were prepared for anodization at 25 V for 6 min in an electrolyte solution (pH 4.7) composed of anhydrous KF, (99.9%, 0.58% mass), $NaHSO_4 \cdot 2H_2O$, (99.9%, 13.8% mass), and trisodium citrate dihydrate ($C_6H_5Na_3O_7 \cdot 2H_2O$, 5.9% mass). An ordered-channel array of anodic titanium oxide (ATO) was obtained and annealed in an air furnace for 3 h at 450°C to form single-crystal nanotubes of anatase ATO. The micromorphology and composition of this anatase ATO were determined with a scanning electron microscope (SEM, JEOL 6500), transmission electron microscope (TEM, JEOL 2100F), energy-dispersive spectrometer (EDS) and X-ray diffraction (XRD, PHILIPS X'Pert Pro).

3 Results and discussion

Figure 1 shows an optical micrograph of an electrolytically polished titanium specimen. The ATO was expected to grow in an ordered-channel array on the flat α-phase titanium surface. Figure 2 shows a SEM image of a spontaneous oxide film of the EP Ti surface. The SEM morphologies of the ATO formed with varied anodizing periods appear in Fig. 3(a)–(i). $Ti(OH)_4$ was initially formed as nanoparticles (a) and nanorods (b) with random distributions. Random nanopores were formed after anodizing for 1.5 min (c). After anodization for 1.5 and 2.5 min, the small pores expanded to diameter 100 nm (d, e). Extra dissolution from the electrolyte required a protracted anodization (f, g, and h). A clean ATO surface shown in Fig. 3(i) was eventually observed after anodization for 6 min.

The SEM morphologies of nanochannel ATO microstructures with long-range order after anodization for 1 h are shown in Fig. 4(a) with a density 10^9–10^{10} tubes cm^{-2}. Figure 4(b) shows the ATO nanostructures with pore size

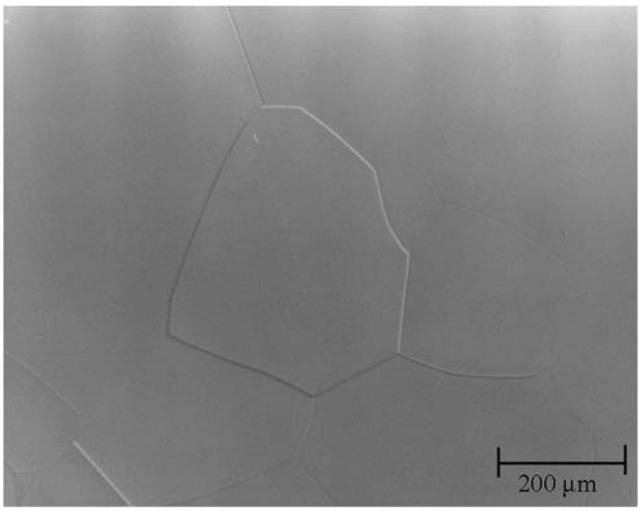

Fig. 1 Optical microscopic image of electro-polished titanium specimen

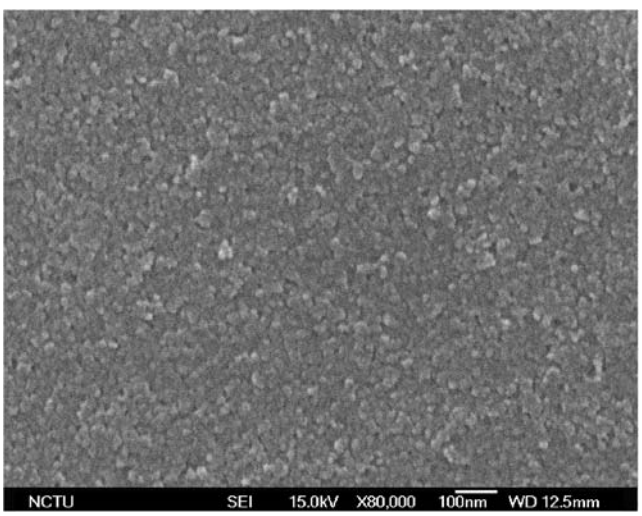

Fig. 2 SEM image of EP Ti surface

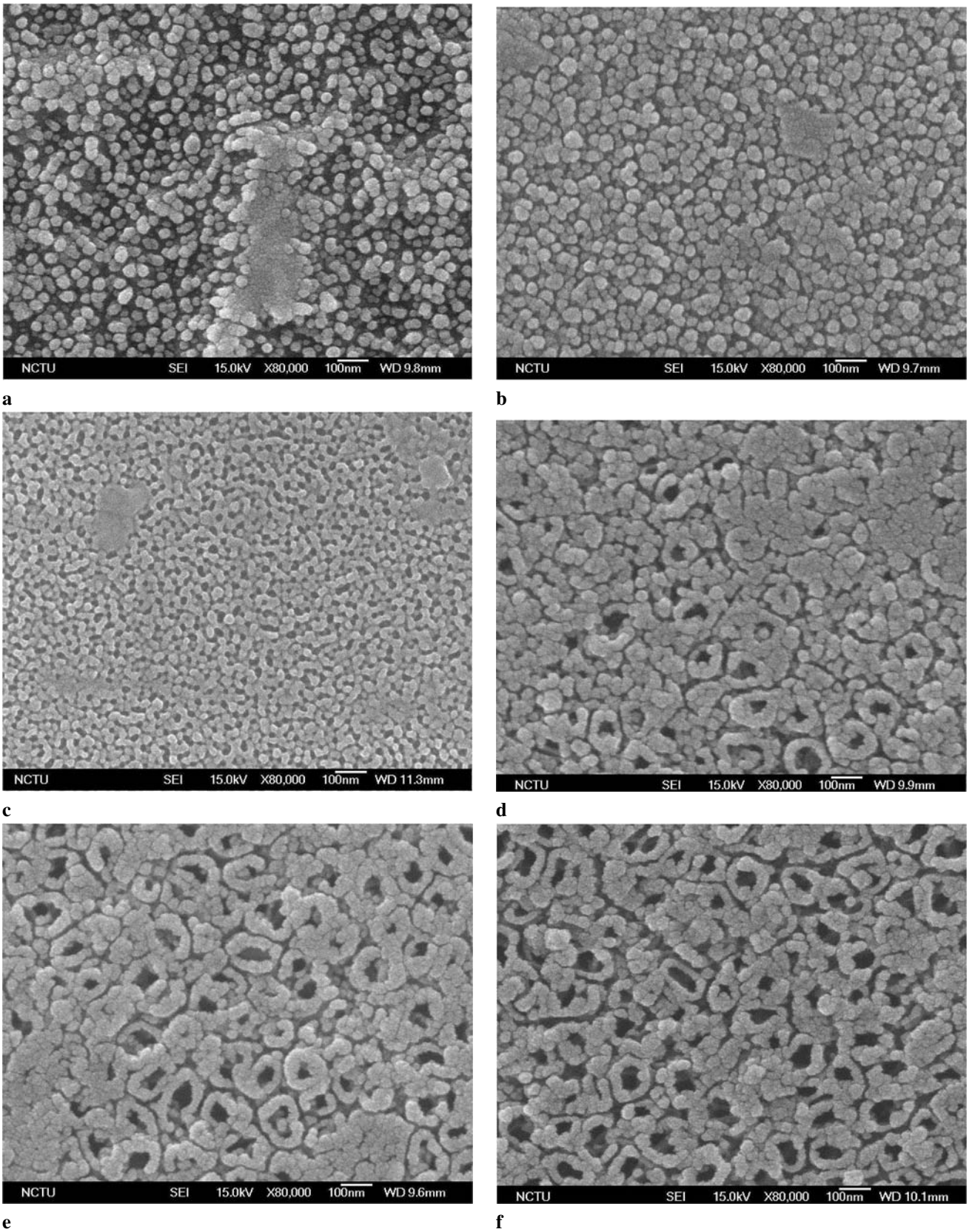

Fig. 3 SEM images of ATO films after anodization for (**a**) 0.5 min, (**b**) 1 min, (**c**) 1.5 min, (**d**) 2 min, (**e**) 2.5 min, (**f**) 3 min, (**g**) 4 min, (**h**) 5 min, (**i**) 6 min

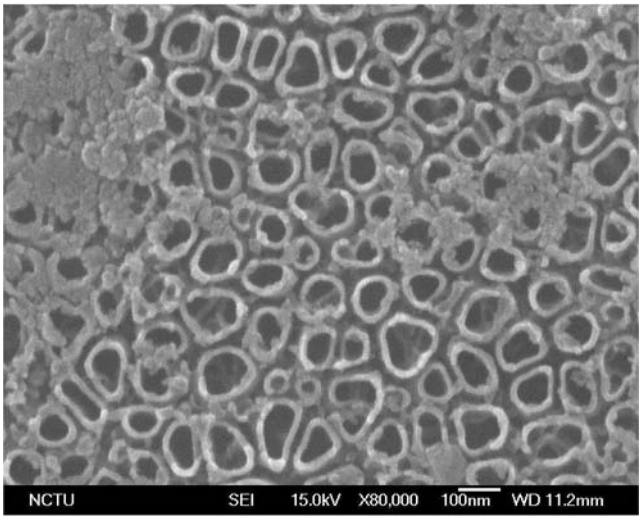

g

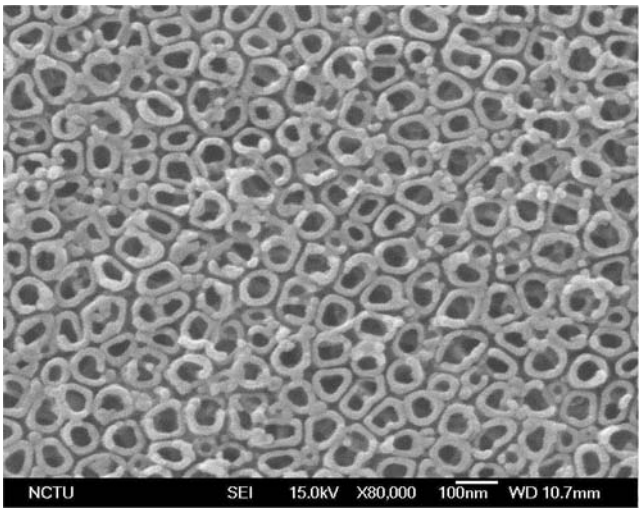

h

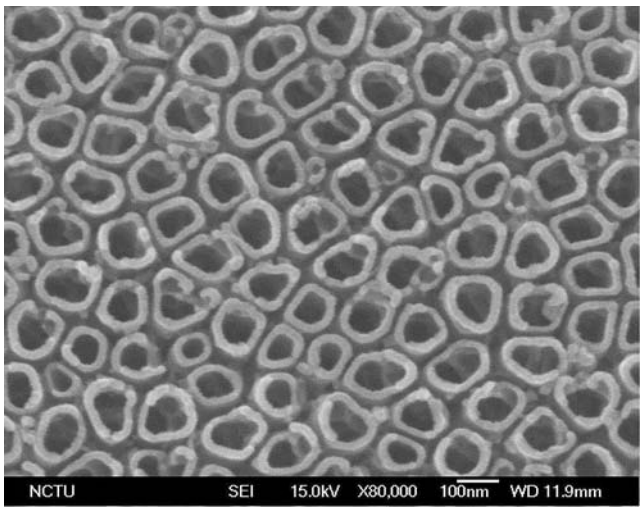

i

Fig. 3 (*Continued*)

100 nm and pore wall thickness 20 nm; Fig. 4(c) shows a tube length 1.5 μm. The barrier layer of closed nanotubes on the bottom of the ATO is shown in Fig. 4(d). The initial phase of the ATO was amorphous and the crystallized anatase TiO_2 was obtained when the amorphous ATO was annealed at 450°C. Figure 5 presents XRD patterns of ATO films on titanium foil; the letters T and A denote α-titanium phase and crystalline anatase, respectively. The titanium phase came from the metallic substrate, which was covered with layers of amorphous TiO_2. TiO_2 features were obtained after annealing for 3 h. Figures 6(a) and 6(b) show typical TEM images and sample ATO diffraction patterns before and after annealing, respectively. A single, randomly selected ATO nanotube was found; it is continuous and has a uniform diameter throughout its length. The observation of free-standing nanotubes in TEM images revealed that most nanotubes were about 3–4 μm long. In Fig. 6(a), the electron diffraction (SAED) pattern in selected areas along the length of the tube indicates a ring pattern (amorphous), but the diffraction patterns in Fig. 6(b) were the same, indicating that the tube was a single crystal. After indexing several SAED patterns from randomly selected nanotubes, the growth direction for some tubes was deduced to be [100]. The XRD shows no single line in the pattern, which indicates that the nanotubes lack the same crystal orientation, but the TEM shows that each individual nanotube is a single-crystal structure.

Figures 7(a) and 7(b) show cross-sectional views of ATO nanochannel arrays on titanium foil for non-annealed (amorphous) and annealed (anatase) TiO_2, respectively. The ATO/Ti interface of the non-annealed specimen presents an ordered pattern with exactly the same morphology as the ATO barrier layer, whereas the interface of the annealed specimen presents a compact layer on the surface with no

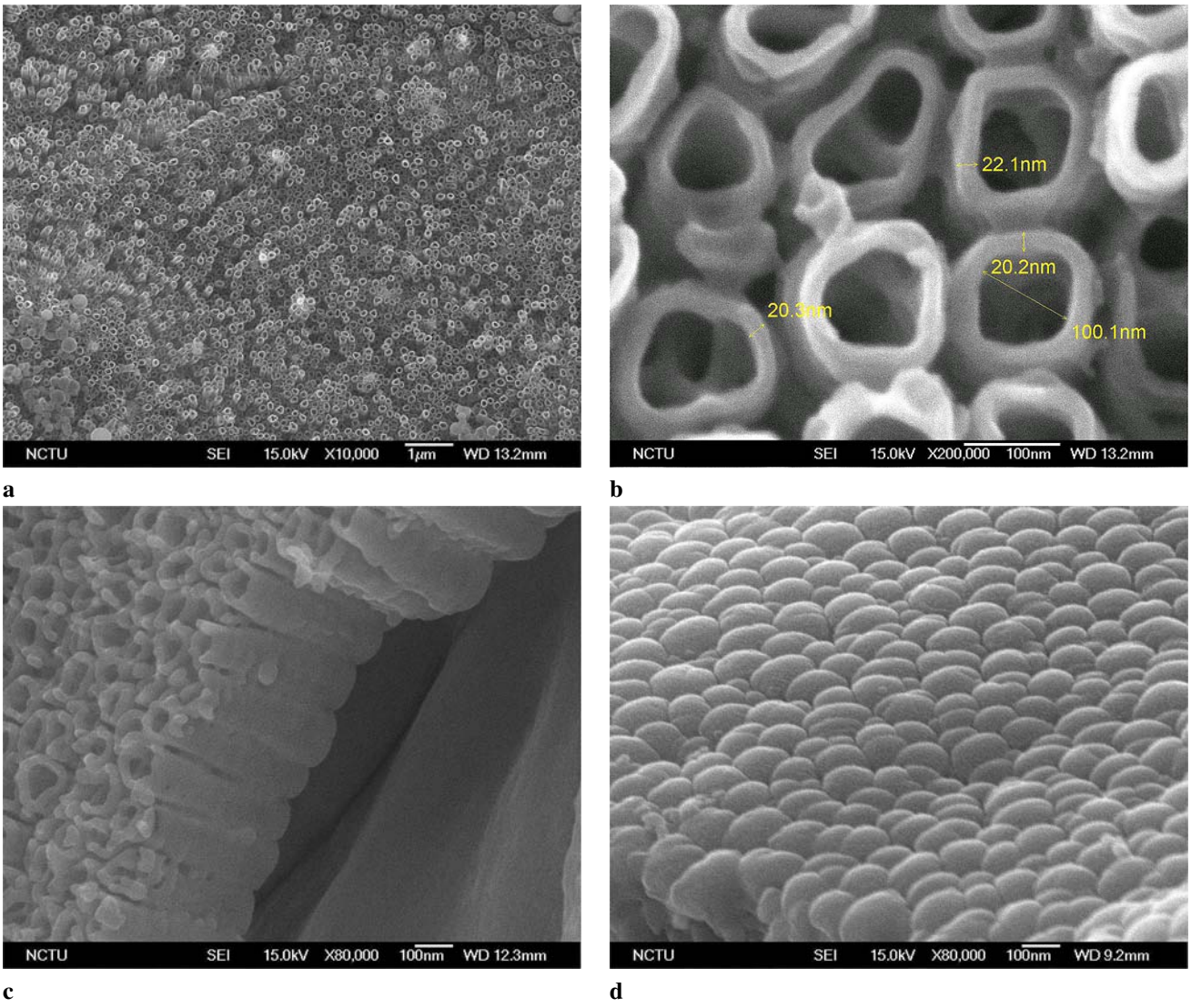

Fig. 4 SEM images of ATO films showing (**a**) tube density 10^9 to 10^{10} cm^{-2}, (**b**) pore size 100 nm and wall thickness 20 nm, (**c**) tube length 1.5 μm, and (**d**) a barrier layer on the bottom of the closed ATO tubes

ordered array. Figure 8 in five parts shows the EDS results of the chemical composition of the thin-film samples shown in Fig. 7. Figure 8(a) indicates that the pattern (point A) is pure Ti, and Fig. 8(b) shows the ATO film (point B) with F doped inside. Figure 8(c) shows that the compact layer (point C) contains a titanium oxide TiO_{2-x} without F doping; Fig. 8(d) shows the composition of the ATO film (point D) with F doping, and Fig. 8(e) shows that the Ti (point E) composition is pure when the compact layer is removed. The departure of TiO_{2-x} from stoichiometry accounts for the vacancies in the oxygen sites.

According to a Ti Pourbaix diagram [28], when Ti is ionized in an electrolyte that contains hydroxide ions, the equilibrium reaction is expressible as

$$TiO^{2+} + 6(OH)^- + 2e^- \rightarrow Ti(OH)_4 + H_{2(g)} + 3O^{2-}. \quad (1)$$

When NH_4F is added to the electrolyte, F^- enters the $(TiOH)_4$ or ATO, and the equilibrium reaction is expressible as

$$TiO^{2+} + 6(OH)^- + 2e^- \xrightarrow{NH_4F} Ti(OH)_{4(F^-\text{doped})} + H_{2(g)} + 3O^{2-}. \quad (2)$$

During anodization, $F_2O_{(g)}$ and $HF_{(g)}$ were formed in the electrolyte [28] and F^- doping to $(TiOH)_4$, and gases $F_{(g)}$, $FO_{(g)}$, $FO_{2(g)}$, $HF_{(g)}$, $H_2F_{2(g)}$, $H_3F_{3(g)}$, $H_4F_{4(g)}$, $H_5F_{5(g)}$, $H_6F_{6(g)}$, and $H_7F_{7(g)}$ were produced [27, 29]. The concentration of F^- in the electrolyte thus decreased for increasing period of anodization. Figure 9 shows the temperature dependence of Gibbs energy for the reactions involving F^-, $F_xO_{y(g)}$, and $H_xF_{y(g)}$; the corresponding expressions for

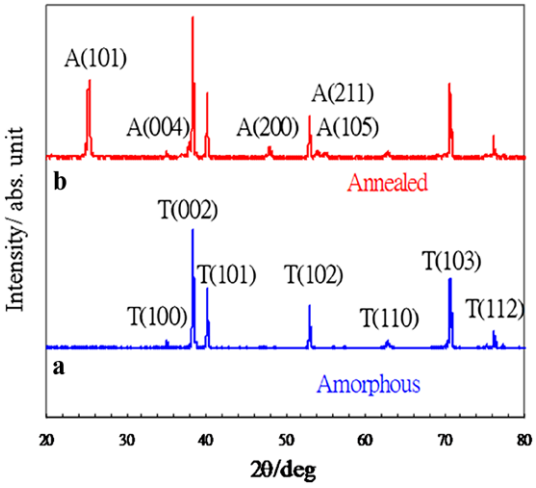

Fig. 5 XRD patterns of (**a**) amorphous ATO grew on a metallic titanium foil; the features were from the α-Ti phase, (**b**) both intense values of α-Ti and anatase phase; T and A represent titanium and anatase, respectively

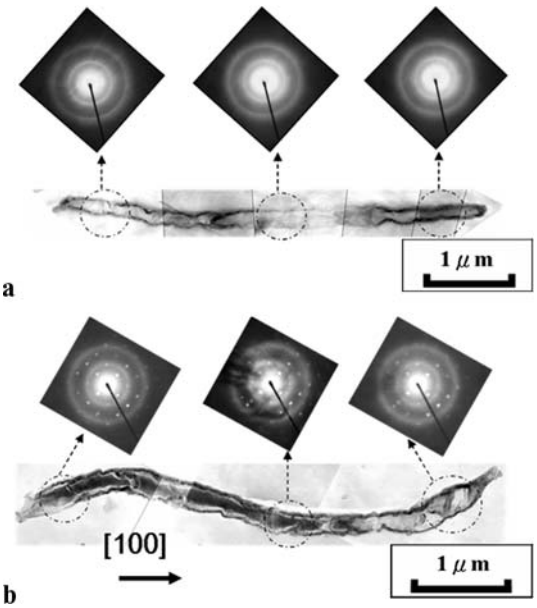

Fig. 6 TEM micrographs of a randomly selected, single TiO_2 nanotube for (**a**) amorphous ATO before annealing, and (**b**) anatase ATO after annealing. The *black circles* indicate the areas from which the electron diffraction (ED) pattern was taken. The zone axis in this case was [112] and the growth direction is [100]

each reaction are listed in Table 1. Accordingly, the gases except $F_{(g)}$, $FO_{(g)}$, and $FO_{2(g)}$ ($\Delta G > 0$) are formed spontaneously during anodization.

The partial vapor pressure of oxygen at equilibrium above the surface of ATO is calculated from the Gibbs energy as follows:

$$TiO_{2(s)} \rightarrow TiO_{2-x(s)} + \frac{x}{2}O_{2(g)}, \tag{3}$$

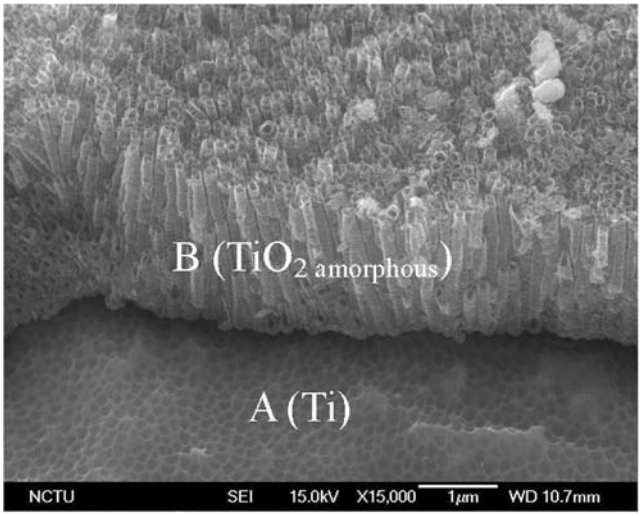

a

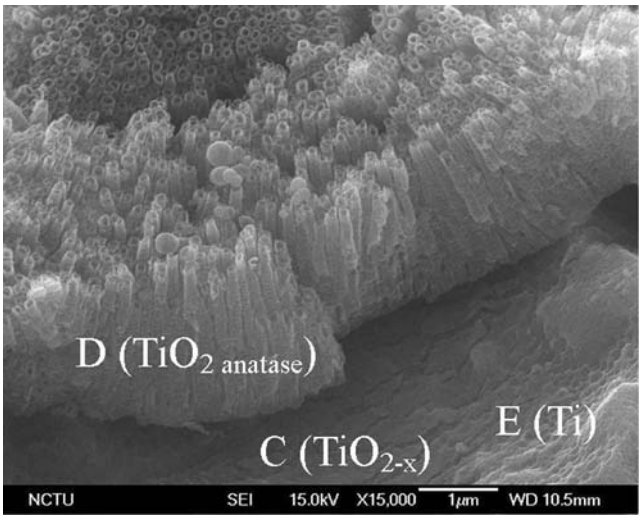

b

Fig. 7 SEM images of ATO/Ti interface showing the interface between Ti substrate and (**a**) amorphous ATO before annealing and (**b**) anatase ATO after annealing

$$\Delta G_1^0 \left(\mathrm{kJ\,mol^{-1}}\right) = -93602 + 0.18T \ (\mathrm{K}). \tag{4}$$

The annealed oxide crystallized and is considered non-stoichiometric if the effect of partial pressure of dioxygen on the composition is significant. The standard molar Gibbs energy change ΔG_1^0 in this reaction is given by

$$\Delta G_1^0 = -RT \ln K_1, \tag{5}$$

in which

$$K_1 = \frac{a_{TiO_{2-x}} \cdot (P_{O_2})^{\frac{x}{2}}}{a_{TiO_2}}. \tag{6}$$

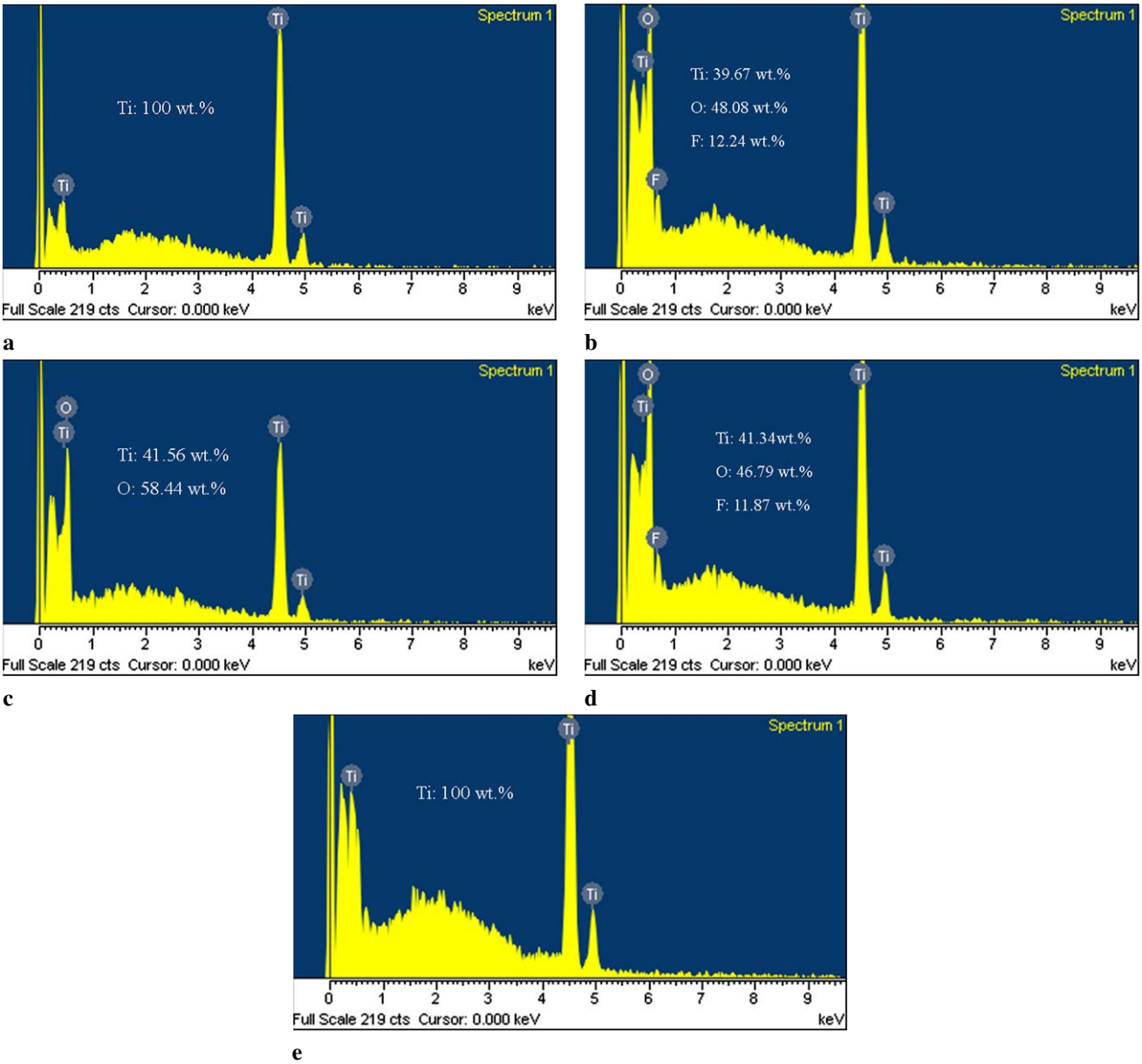

Fig. 8 EDS of ATO films in locations labeled in Fig. 7 for (**a**) pure Ti, (**b**) TiO_2 with F doping, (**c**) TiO_{2-x} without F doping, (**d**) TiO_2 with F doping, and (**e**) pure Ti

If the activities of solid compounds are assumed to be unity, on combining (5) with (6) we obtain

$$(P_{O_2})^{\frac{x}{2}} = \exp\left(\frac{-\Delta G_1^0}{RT}\right). \tag{7}$$

Based on the Ti–O binary phase diagram [30] with $x = 2.0$, 1.75, 1.67, 1.5 and 1.0, the partial pressures of dioxygen for air/TiO_2, TiO_2/Ti_4O_7, Ti_4O_7/Ti_3O_5, Ti_3O_5/Ti_2O_3, Ti_2O_3/TiO, and TiO/Ti at 450°C are $10^{-0.7}$, $10^{-43.11}$, $10^{-45.15}$, $10^{-47.21}$, $10^{-53.49}$ and $10^{-68.22}$ atm, respectively. Table 2 summarizes the results for $\log K$, ΔG^0, and $\log P_{O_2}$ based on the JANAF thermochemical table [27]. Table 3 lists equilibrium states of dioxygen at partial pressures and various temperatures with a schematic illustration displayed in Fig. 10.

It is convenient to express a reaction using the Kroger–Vink notation [31] as

$$2V_{Ti} + V_O = 2V_{Ti'} + V_{O^{\cdot\cdot}} + \frac{1}{2}O_{2(g)}, \tag{8}$$

which is equivalent to

$$V_O = V_{O^{\cdot\cdot}} + \frac{1}{2}O_{2(g)} + 2e^-. \tag{9}$$

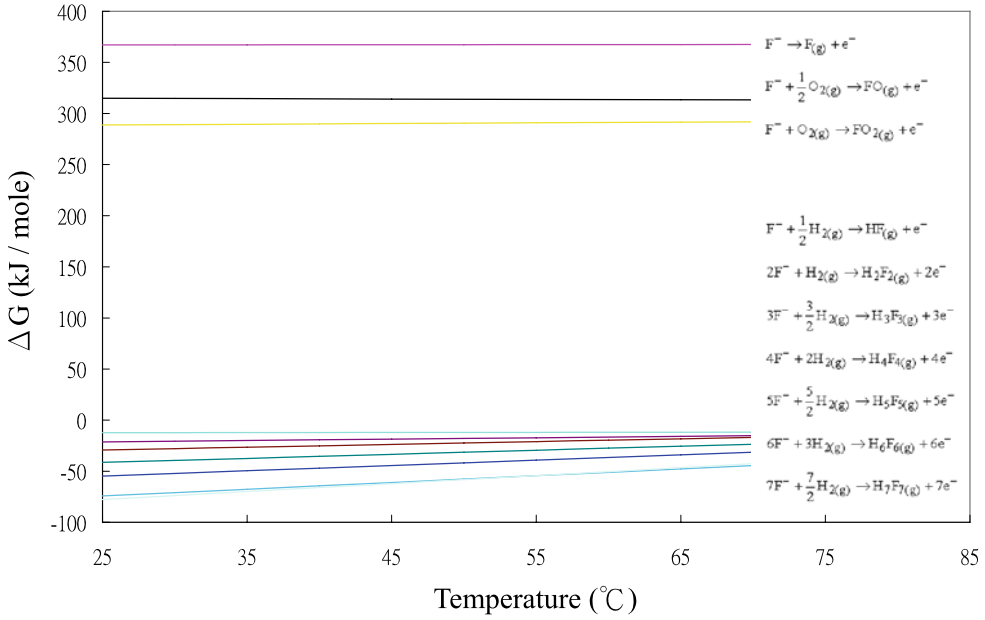

Fig. 9 Diagram of Gibbs energy of reaction. Values for $F_{(g)}$, $FO_{(g)}$, $FO_{2(g)}$ are positive but those for $HF_{(g)}$, $H_2F_{2(g)}$, $H_3F_{3(g)}$, $H_4F_{4(g)}$, $H_5F_{5(g)}$, $H_6F_{6(g)}$, and $H_7F_{7(g)}$ are negative; the latter species can spontaneously form during anodization

Table 1 Gibbs energy of reactions involving F^-, $F_xO_{y(g)}$, and $H_xF_{y(g)}$

No.	Reactions	ΔG (kJ mol^{-1})
1	$F^- \rightarrow F_{(g)} + e^-$	$325.63 - 0.036T$
2	$F^- + \frac{1}{2}O_{2(g)} \rightarrow FO_{(g)} + e^-$	$364.13 + 0.01T$
3	$F^- + O_{2(g)} \rightarrow FO_{2(g)} + e^-$	$267.93 + 0.07T$
4	$F^- + \frac{1}{2}H_{2(g)} \rightarrow HF_{(g)} + e^-$	$-16.57 + 0.014T$
5	$2F^- + H_{2(g)} \rightarrow H_2F_{2(g)} + 2e^-$	$-61.24 + 0.134T$
6	$3F^- + \frac{3}{2}H_{2(g)} \rightarrow H_3F_{3(g)} + 3e^-$	$-111.51 + 0.276T$
7	$4F^- + 2H_{2(g)} \rightarrow H_4F_{4(g)} + 4e^-$	$-160.03 + 0.398T$
8	$5F^- + \frac{5}{2}H_{2(g)} \rightarrow H_5F_{5(g)} + 5e^-$	$-209.75 + 0.52T$
9	$6F^- + 3H_{2(g)} \rightarrow H_6F_{6(g)} + 6e^-$	$-271.52 + 0.662T$
10	$7F^- + \frac{7}{2}H_{2(g)} \rightarrow H_7F_{7(g)} + 7e^-$	$-310.16 + 0.787T$

The equilibrium quotient of (8) is given by

$$K = [V_{O^{\cdot\cdot}}] \cdot (P_{O_2})^{\frac{1}{2}} \cdot [e^-]/[V_O], \tag{10}$$

in which V_{Ti} and V_O are the vacancies at Ti and O sites, respectively; $V_{O^{\cdot\cdot}}$ and $V_{Ti'}$ are the excess oxygen charge and titanium charge located at the vacant sites, respectively. The concentration of oxygen in ATO is expressed as [Oo], which signifies that the interstitial or substituted oxygen at the original site of oxygen from substrates is near unity, and the concentration of electrons equals twice the oxygen vacancies, i.e., $2[V_{O^{\cdot\cdot}}] = [e^-]$; $[V_{O^{\cdot\cdot}}]$ is approximately equal to the negative one-sixth power of the oxygen partial pressures, i.e., $\sim(PO_2)^{-1/6}$. This relation is consistent with the Brouwer approximation [32], which indicates the strong influence of stoichiometry and the expected dependence of oxygen pressure on defect structure.

The order of Ti/O is evaluated through the oxygen pressure of the oxide/metal interface. The driving force in growing anatase ATO nanotubes is drawing oxygen from the atmosphere to the oxygen site (Oo); i.e., (8) shifts to the left, and the concentration of oxygen vacancies during crystal growth becomes decreased. Conversely, as the reductive potential occurs toward the interfaces of the titanium substrate, the concentration of oxygen vacancies increases, and (8) shifts to the right. Because of the small ionization energy of titanium ions, an extensive non-stoichiometric region in (8) is predominant inside the entire ATO layers.

4 Conclusions

Anodic titanium oxide (ATO) film with pore diameter 100 nm, density 10^9 to 10^{10} tubes cm^{-2}, and nanochannel array of length 1.5 μm was fabricated through anodization. Crystalline nanotubes of ATO were obtained on annealing the amorphous form at high temperature. Because oxygen was introduced into the interface between substrate Ti and ATO during annealing, oxide layers of TiO_{2-x} were formed. Annealing yielded an equilibrium distribution to states of energy that increased the probability of electrons overcoming the energy level within ATO. Based on thermodynamic considerations, the compositions of the oxide layers above the Ti surface were determined to be TiO, Ti_2O_3, Ti_3O_5, Ti_4O_7 and TiO_2. The calculated partial pressures at the interfaces air/TiO_2, TiO_2/Ti_4O_7, Ti_4O_7/Ti_3O_5, Ti_3O_5/Ti_2O_3, Ti_2O_3/TiO and TiO/Ti at 450°C are $10^{-0.7}$, $10^{-43.11}$, $10^{-45.15}$, $10^{-47.21}$, $10^{-53.49}$, and $10^{-68.22}$ atm, respectively. The evidence from

Table 2 Equilibrium reaction equations for Ti/O in the temperature range 25–500°C

Reaction	log K	ΔG/kJ	log (P_{O_2}/atm)
$Ti + O_2 \rightarrow TiO_{2(A)}$	$\log K = -9.394 + \frac{4885.7}{T}$	$\Delta G = -93602 + 0.18T$	$\log P_{O_2}(\text{atm}) = -\log K$
$4Ti + \frac{7}{2}O_2 \rightarrow Ti_4O_7$	$\log K = -32.163 + \frac{177194.3}{T}$	$\Delta G = -3392.74 + 0.62T$	$\log P_{O_2}(\text{atm}) = -\frac{2}{7}\log K$
$3Ti + \frac{5}{2}O_2 \rightarrow Ti_3O_5$	$\log K = -23.723 + \frac{127944.3}{T}$	$\Delta G = -2449.74 + 0.45T$	$\log P_{O_2}(\text{atm}) = -\frac{2}{5}\log K$
$2Ti + \frac{3}{2}O_2 \rightarrow Ti_2O_3$	$\log K = -14.14 + \frac{78926.6}{T}$	$\Delta G = -1511.21 + 0.27T$	$\log P_{O_2}(\text{atm}) = -\frac{2}{3}\log K$
$4Ti + \frac{1}{2}O_2 \rightarrow TiO$	$\log K = -4.97 + \frac{28262.3}{T}$	$\Delta G = -541.14 + 0.09T$	$\log P_{O_2}(\text{atm}) = -2\log K$

Table 3 Oxygen partial pressures for each Ti/O equilibrium state at 450°C

Interface	Reactions	log (P_{O_2}/atm)
Air/TiO_2	–	−0.7
TiO_2/Ti_4O_7	$TiO_2 + 4Ti + 2.5O_2 \rightarrow Ti_4O_7$	−43.11
Ti_4O_7/Ti_3O_5	$Ti_4O_7 \rightarrow Ti_3O_5 + Ti + O_2$	−45.15
Ti_3O_5/Ti_2O_3	$Ti_3O_5 \rightarrow Ti_2O_3 + Ti + O_2$	−47.21
Ti_2O_3/TiO	$Ti_2O_3 \rightarrow TiO + Ti + O_2$	−53.49
TiO/Ti	$TiO \rightarrow Ti + 0.5O_2$	−68.22

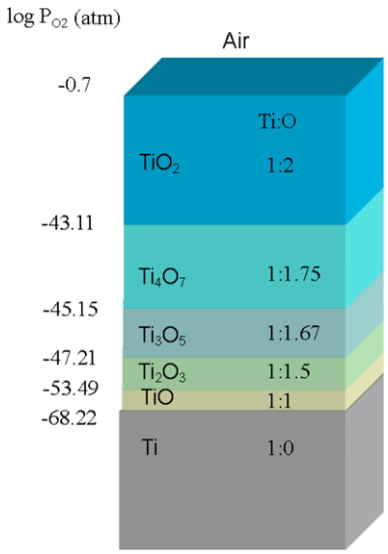

Fig. 10 Schematic illustration of metal-oxide layers above titanium foil with the equilibrium oxygen partial pressures at the interface

EDS and the expected dependence of oxygen pressure on defect structure clearly demonstrates the non-stoichiometric structures of the crystalline ATO layers. The driving force of growing crystalline ATO nanotubes is to gain oxygen from the atmosphere to the oxygen site. The oxygen vacancy concentration is approximately equal to the negative of one sixth power of oxygen partial pressures, consistent with the Brouwer approximation. Because of the small ionization energy of titanium ions, an extensive region of non-stoichiometric defects is expected in the ATO layers.

Acknowledgements National Science Council of Taiwan (contracts 96-2628-M-009-018-MY2 and 97-3114-M-009-093-) and the MOE-ATU program provided financial support.

References

1. J. Zhao, X. Wang, T. Sun, L. Li, Nanotechnology **16**, 2450 (2005)
2. H. Shin, D.K. Jeong, J. Lee, M. Sung, J. Kim, Adv. Mater. **16**, 1197 (2004)
3. C.C. Chen, Y. Bisrat, Z.P. Luo, R.E. Schaak, C.G. Chao, D.C. Lagoudas, Nanotechnology **17**, 367 (2006)
4. H. Masud, K. Fukuda, Science **268**, 1466 (1995)
5. H. Tsuchiya, J.M. Macak, L. Taveira, P. Schmuki, Chem. Phys. Lett. **410**, 188 (2005)
6. I. Sieber, H. Hildebrand, A. Friedrich, P. Schmuki, Electrochem. Commun. **7**, 97 (2005)
7. H.C. Shin, J. Dong, M. Liu, Adv. Mater. **16**, 237 (2004)
8. H. Tsuchiya, J.M. Macak, I. Sieber, L. Taveira, A. Ghicov, K. Sirotna, P. Schmuki, Electrochem. Commun. **7**, 295 (2005)
9. H. Tsuchiya, P. Schmuki, Electrochem. Commun. **7**, 49 (2005)
10. G.K. Mor, K. Shankar, M. Paulose, O.K. Varghese, C.A. Grimes, Nano Lett. **6**, 215 (2006)
11. H. Yamashita, Y. Ichihashi, Appl. Surf. Sci. **121**, 305 (1997)
12. A.M. Azad, S.A. Akbar, J. Electrochem. Soc. **139**, 3690 (1992)
13. C.C. Chen, J.S. Lin, E.W.G. Diau, T.F. Liu, Appl. Phys. A **92**, 615 (2008)
14. C.C. Chen, H.W. Chung, C.H. Chen, H.P. Lu, C.M. Lan, S.F. Chen, L. Luo, C.S. Hung, E.W.G. Diau, J. Phys. Chem. C **112**, 19151 (2008)
15. K. Zhu, N.R. Neale, A. Miedaner, A.J. Frank, Nano Lett. **7**, 69 (2007)
16. K. Shankar, G.K. Mor, H.E. Prakasam, S. Yoriya, M. Paulose, O.K. Varghese, C.A. Grimes, Nanotechnology **18**, 065707 (2007)
17. C.C. Chen, J.H. Chen, C.G. Chao, W.C. Say, J. Mater. Sci. **40**, 4053 (2005)
18. V. Zwilling, M. Aucouturier, E. Darque-Ceretti, Electrochim. Acta **45**, 921 (1999)
19. D. Gong, C.A. Grimes, O.K. Varghese, Z. Chen, W.C. Hu, E.C. Dickey, J. Mater. Res. **16**, 3331 (2001)
20. Q. Cai, M. Paulose, O.K. Varghese, C.A. Grimes, J. Mater. Res. **20**, 230 (2005)
21. C.A. Grimes, J. Mater. Chem. **17**, 1451 (2007)
22. J.M. Macak, H. Tsuchiya, L. Taveira, S. Aldabergerova, P. Schmuki, Angew. Chem. Int. Ed. **44**, 7463 (2005)
23. M. Paulose, K. Shankar, S. Yoriya, H.E. Prakasam, O.K. Varghese, G.K. Mor, T.A. Latempa, J. Phys. Chem. B **110**, 16179 (2006)
24. M. Paulose, H.E. Prakasam, O.K. Varghese, L. Peng, K.C. Popat, G.K. Mor, T.A. Desai, C.A. Grimes, J. Phys. Chem. C **111**, 14992 (2007)
25. O.K. Varghese, D. Gong, M. Paulose, C.A. Grimes, E.C. Dickey, J. Mater. Res. **18**, 156 (2003)

26. A.G. Mantzila, M.I. Prodromidis, Electrochimica Acta **51**, 3537 (2006)
27. Syverud, JANAF Thermochemical Table, 3rd. ed., J. Phys. Chem. Ref. Data (1985)
28. M. Pourbaix, Texas/National Association of Corrosion Engineers, Houston, USA (1974)
29. I. Barin, *Thermochemical Data of Pure Substances* (VCH, Weinheim, 1989)
30. J.L. Murray, *Phase Diagrams of Binary Titanium Alloys* (ASM International, Materials Park, 1985), p. 211
31. W.D. Kingery, H.K. Bowen, D.R. Uhlmann, *Introduction to Ceramics* (Wiley, New York, 1975), p. 127
32. M. Barsoum, *Fundamentals of Ceramics* (McGraw-Hill, New York, 1997), p. 172